Ligand Migration in Nonsymbiotic Hemoglobin AHb1 from *Arabidopsis thaliana*

Stefania Abbruzzetti,[†] Elena Grandi,[†] Stefano Bruno,[‡] Serena Faggiano,[‡] Francesca Spyrakis,[‡,§] Andrea Mozzarelli,[‡] Elena Cacciatori,[||] Paola Dominici,[||] and Cristiano Viappiani*[,†]

Dipartimento di Fisica, Università degli Studi di Parma, NEST CNR-INFM, Parma, Italy, Dipartimento di Biochimica e Biologia Molecolare, Università degli Studi di Parma, Parma, Italy, Dipartimento Scientifico e Tecnologico, Università degli Studi di Verona, Verona, Italy, and INBB, Biostructures and Biosystems National Institute, Roma, Italy

Received: June 26, 2007; In Final Form: August 27, 2007

AHb1 is a hexacoordinated type 1 nonsymbiotic hemoglobin recently discovered in *Arabidopsis thaliana*. To gain insight into the ligand migration inside the protein, we studied the CO rebinding kinetics of AHb1 encapsulated in silica gels, in the presence of glycerol. The CO rebinding kinetics after nanosecond laser flash photolysis exhibits complex ligand migration patterns, consistent with the existence of discrete docking sites in which ligands can temporarily be stored before rebinding to the heme at different times. This finding may be of relevance to the physiological NO dioxygenase activity of this protein, which requires sequential binding of two substrates, NO and O_2, to the heme.

Introduction

The dynamics of proteins is critical to their function, and the understanding of the modulation mechanisms at a detailed molecular level is still one of the most relevant issues of biophysics. While new members are being continuously added to the hemoglobins family,[1−4] myoglobin (Mb) and hemoglobin (Hb) continue to be used as model protein systems to understand how structure and dynamics contribute to the protein function. Among other methods, the rebinding of diatomic ligands following laser photolysis has been extensively used over the years to understand the molecular mechanisms underlying protein−ligand interactions and to establish physiological functions of newly discovered hemoglobins.

When ligand recombination is investigated at cryogenic temperatures, the observed kinetics indicate the existence of a frozen distribution of functionally distinct conformational substates.[5,6] As the temperature is raised, thermal averaging of the conformational substates cancels the kinetic hole burning phenomena[7] observed at lower temperatures[8,9] and new kinetic phases are observed,[5,6,10−13] which apparently lead to an inverse temperature effect of the observed kinetics. Different explanations were offered for the observed anomalous temperature dependence. These included the existence of barrier raising conformational relaxations[14−17] and the existence of routes leading to slowly rebinding, temporary docking sites.[18,19] The temporary docking sites were subsequently identified in myoglobin as the packing defects referred to as xenon cavities.[20−29] Therefore, the discrete kinetic phases of ligand rebinding upon flash photolysis received a new structural interpretation as due to the existence of kinetic traps for the photodissociated ligands.[30−40] However, the involvement of protein dynamics is not excluded within this frame, and a model merging the structural view with the existence of an overlapped modulation by protein dynamics was recently proposed for myoglobin.[41] The spectroscopic evidence of structural relaxation signatures was reported in the transient absorbance signals following photolysis[10,17,42,43] and recently confirmed also from time-resolved X-ray crystallography data on myoglobin mutants.[28,44]

The presence of internal cavities and packing defects has recently emerged as one of the general strategies that small globular proteins use to perform their function.[45] The reduction in thermodynamic stability that such a structure might cause appears to be more than compensated by the capability of controlling ligand diffusion to the active site through the matrix, possibly by transiently storing more than one reactant at a time.[46] The fraction of photodissociated ligands which are rebound within the protein matrix (i.e., before they escape to solution) reflects both ligand migration and protein dynamics. To make the geminate phase more informative, while still preserving the kinetic energy associated with thermal motion at room temperature, it has become popular to embed proteins in silica gels,[47] possibly in the presence of viscogenic agents as glycerol[38,40,48−57] or trehalose glasses.[33,34,39,41,58] Under these experimental conditions the geminate phase is normally enhanced. Gel encapsulation and increased viscosity both favor otherwise thermodynamically unstable states such as those associated with the ligand inside the protein matrix.[38,48−53]

The recently discovered nonsymbiotic hemoglobin AHb1 from *Arabidopsis thaliana* shows a nonexponential and weakly temperature-dependent geminate rebinding upon flash photolysis of its CO complex. This fast process exhibits a very small amplitude with respect to the bimolecular rebinding, involving the migration of the ligand from the bulk solution.[53,59] The ligand binding was shown to be partly regulated by the competing binding of the distal HisE7, which normally forms a sixth coordination bond with the heme iron, in the absence of exogenous ligands, both in the ferric and in the ferrous states. The rebinding is probably also regulated by the complex system of internal hydrophobic cavities that was revealed by an analysis

* To whom correspondence should be addressed. E-mail: cristiano.viappiani@fis.unipr.it. Tel.: +390521905208. Fax: +390521905223.

[†] Dipartimento di Fisica, Università degli Studi di Parma and NEST CNR-INFM, Italy.

[‡] Dipartimento di Biochimica e Biologia Molecolare, Università degli Studi di Parma.

[§] INBB.

[||] Dipartimento Scientifico e Tecnologico, Università degli Studi di Verona.

10.1021/jp074954o CCC: $37.00
Published on Web 10/09/2007

of the three-dimensional structure model obtained by homology modeling.[59] In particular, an apolar tunnel connects the distal cavity with the solvent, and is possibly responsible for the observed small geminate recombination.[59] Similar structural features, previously reported for human[60] and murine[61] neuroglobins and bacterial truncated hemoglobins,[3] were recently postulated to have functional significance in the NO dioxygenase activity of these proteins on the basis of experimental data[1,62] and molecular dynamics simulations.[63] AHb1 was shown to have a NO dioxygenase activity in vitro and to reduce levels of NO under hypoxic stress.[64] Biochemical evidence indicates that rapid nitrate accumulation is accompanied by NO-dependent oxidation of oxygenated to oxidized AHb1. Furthermore, this Fe^{3+} intermediate of heme can be directly reduced by NADPH, which supports continuous nitrate accumulation in the presence of excess NO. Otherwise, oxidized nsHb might be reduced by a mixture of NADH and FAD or by a methemoglobin reductase.[65]

It is therefore important to characterize ligand migration processes that may help gaining mechanistic insight into the physiological NO dioxygenase activity of this protein, which requires sequential binding of two substrates, NO and O_2, to the heme.

In this work we have encapsulated the CO complex of AHb1 in silica gel and characterized the ligand rebinding kinetics after nanosecond laser photolysis when gels are soaked in glycerol. We show that under the high viscosity conditions employed in this work the rebinding kinetics is consistent with migration of CO to discrete docking sites where it becomes trapped. The observed pattern for the different microscopic rates associated with each process reflects the presence of an internal viscosity effect, as previously evidenced for Mb.[16,17,50]

Experimental Methods

Samples Preparation. AHb1 was cloned, expressed, and purified as described elsewhere.[59]

For experiments in solution, concentrated stock solutions of AHb1 were diluted in 100 mM sodium phosphate buffer and 1 mM EDTA, pH 7.0, to a final concentration ranging from 60 to 70 μM. Before the experiments, the solutions were equilibrated with nitrogen/CO mixtures of known CO partial pressure and sodium dithionite was added to a concentration of 2 mM to prevent oxidation.

The encapsulation of AHb1 in silica gels was carried out by following the protocol reported by Shibayama and Saigo[66] with some modifications. A solution containing tetramethyl orthosilicate, water, and hydrochloric acid was sonicated for 20 min at 4 °C. An equal volume of a deoxygenated solution containing 10 mM phosphate, pH 6.0, was then added to the sol, which was further deoxygenated for 40 min at 4 °C under a flux of nitrogen. Finally, a 200 μM solution of AHb1 in 50 mM phosphate buffer at pH 7.2, equilibrated with a 1 atm CO, was anaerobically added to the sol. The resulting mixture was layered on quartz plates under anaerobic conditions. Gelation occurred in approximately 20 min. The silica wet gels were anaerobically stored for at least 3 days in a buffer containing 100 mM phosphate, 1 mM EDTA, and 5 mM sodium dithionite, pH 7.0 at 4 °C. The protein concentration in the gel was approximately 110 μM. Before the experiments, the gels were anaerobically transferred in a solution previously equilibrated with a CO/nitrogen mixture of known CO partial pressure. In the case of experiments carried out in aqueous solutions, gels were soaked in a 100 mM phosphate buffer, 1 mM EDTA, and 2 mM sodium dithionite, pH 7.0. For experiments under high-viscosity conditions, gels were transferred to 100% glycerol and equilibrated for at least 3 days at 4 °C.

Microspectrophotometry of AHb1 Gels. Absorption spectra of COAHb1 gels were carried out using a Zeiss MPM03 microspectrophotometer, equipped with a ×10 UV−visible Ultrafluar objective.[67,68] The gel was anerobically loaded on a Dvorak-Stotler flow cell in the presence of sodium dithionite and kept under flux of helium throughout the experiments. Spectra were collected in the 380−700 nm range. Photolysis of the CO complex was carried out by shining white light on the sample immediately before spectra acquisition.

Laser Flash Photolysis Setup. The experimental setup was described in detail elsewhere.[53] Photolysis of CO complexes was obtained by using the second harmonic (532 nm) of a Q-switched Nd:YAG laser, either a Surelite II-10 (Continuum) or a Handy Yag HYL-101 (Quanta System). The linear polarization is converted to circular by a quarter waveplate to minimize photoselection effects. Near-full photolysis is normally obtained with the setups described below, with laser pulses of 20−40 mJ, depending on the sample.

The absorbance changes are monitored using a monochromatic cw output of a 150 W Xe arc lamp coupled to a 0.25-m monochromator (AMKO GmBH). The transient absorbance traces are measured through a second, 0.125-m monochromator (77250, LOT-Oriel) with a 5 stages photomultiplier (PMT) (Applied Photophysics). The voltage signal is digitized by a digital oscilloscope (LeCroy LT374, 500 MHz, 4 GS/s). A custom dichroic filter (Omega optical) is positioned between the exit slit of the monochromator and the photomultiplier to remove the residual stray light from the pump laser. A fast shutter (Vincent Associates, Uniblitz VS35) is positioned between the output of the first monochromator and the sample holder. The opening of the shutter is controlled by a dedicated microprocessor,[69] while exposure time is set by the shutter driver (Vincent Associates, Uniblitz VMM-T1). The sample holder is accurately temperature controlled with a Peltier element, allowing a temperature stability better than 0.1 °C. Rebinding kinetics after photolysis of the CO complexes were measured at seven temperatures between 10 and 40 °C and at three CO partial pressures, 1, 0.1, and 0 atm (nitrogen-saturated bathing solutions).

Data Analysis. To highlight the number and the relative roles of the different kinetics phases, the lifetime distributions associated with the observed kinetics were evaluated using the program MemExp (version 3.0) written by P. J. Steinbach.[70,71] The program MemExp uses the maximum entropy method (MEM) and either nonlinear least-squares (NLS) or maximum likelihood (ML) fitting to analyze a general time-dependent signal in terms of distributed and discrete lifetimes. One distribution of effective log-lifetimes, $g(\log \tau)$, was extracted from the experimental data.

$$\mathcal{T}_i = D_0 \int_{-\infty}^{+\infty} g(\log(\tau)) e^{-ti/\tau}\, \mathrm{d}(\log \tau) + \sum_{k=0}^{3} (b_k - c_k)(t_i/t_{\max})^k \quad (1)$$

The polynomial describes the baseline. The $g(\log(\tau))$ distribution is obtained numerically from the data and is not restricted to any functional form. MemExp automatically recommends one distributed description of the kinetics as optimal. Baselines were always flat and of very small amplitude. The quality of the fits was always excellent, with the residuals randomly oscillating around zero.

The analysis of the CO rebinding kinetics measured for glycerol soaked AHb1 gels required the use of differential blurring[70,71] to reproduce the steep phase on the short time scale.

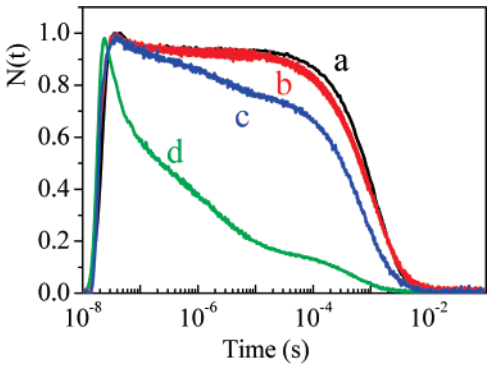

Figure 1. Comparison between the CO rebinding kinetics after photolysis of COAHb1 solutions (black curve, a) and COAHb1 gels soaked in a buffered solution (red curve, b), in 80% glycerol (blue curve, c) and in 100% glycerol (green curve, d). All displayed curves were measured at $T = 10$ °C and 1 atm CO.

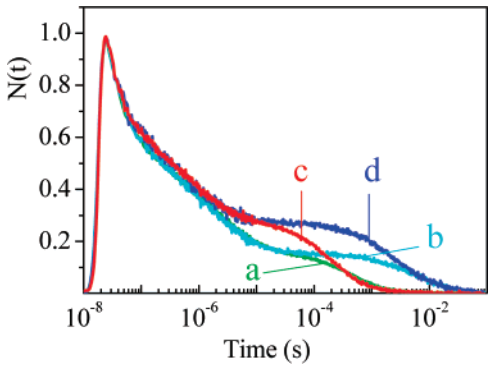

Figure 2. Comparison between the CO rebinding kinetics after photolysis of COAHb1 gels soaked in 100% glycerol at $T = 10$ °C (a, green curve, 1 atm CO; b, cyan curve, N_2 saturated) and at $T = 40$ °C (c, red curve, 1 atm CO; d, blue curve, N_2 saturated).

The differential equations associated with the tested kinetic schemes were solved numerically, and the rate constants appearing in the equilibrium were optimized to obtain the best fit to the experimental data. Numerical solutions to the set of coupled differential equations associated with reaction schemes were determined by using the function ODE15s within Matlab 7.0 (The MathWorks, Inc.). Fitting of the numerical solution to experimental data was obtained with a Matlab version of the optimization package Minuit (CERN).

To improve the capability of retrieving the microscopic rate constants, data at different CO concentrations at the same temperature were simultaneously fitted. We analyzed rebinding kinetics for COAHb1 gels soaked in solutions equilibrated with three different CO partial pressures (1, 0.1, and 0 atm, corresponding to a solution saturated with pure nitrogen). Additional details of the method can be found in previous publications.[53,59] This global analysis was repeated at seven different temperatures between 10 and 40 °C. From the temperature dependence of the microscopic rate constants, we estimated activation energies using Arrhenius plots, which were linear. A modified Kramers equation was used to highlight the contribution of viscosity to the recovered microscopic rates.[16,72]

Results and Discussion

The effect of gel encapsulation on the ligand rebinding kinetics to AHb1 is relatively small,[53] as can be appreciated from the comparison, in Figure 1, between the ligand rebinding kinetics in solution and in the gel soaked in an aqueous buffered solution. The amplitude and the apparent rate of the geminate phase in the gel are very similar to the corresponding values observed in solution at the same temperature and CO partial pressure. The only remarkable effects appear in the slow phase, where the competition between the internal His and the exogenous ligand is mostly evident.[53] Steady-state spectroscopic investigations on both Fe^{2+} and Fe^{3+} deoxy AHb1 solutions showed that HisE7 (the distal His residue) is completing the heme Fe coordination.[59] CO rebinding kinetics showed that the endogenous HisE7 ligand is capable of competing with CO in binding to the Fe on the millisecond time scale, although with a low efficiency.[59] When CO rebinding kinetics to COAHb1 gels is measured, the endogenous ligand is more efficient in the competitive reaction and leads to a broadening of the second-order rebinding kinetics, due to increased ligation/dissociation rates of HisE7 in comparison with what is observed in solution.[53,73]

Figure 1 also compares the rebinding kinetics for gels soaked in 80% and in 100% glycerol. The rebinding kinetics shows a kinetic pattern of progressively increasing complexity, characterized by higher rebinding rates as the glycerol concentration is increased. Figure 2 reports representative rebinding kinetics at 10 and 40 °C for AHb1 gels soaked in 100% glycerol measured at 1 atm CO and in nitrogen saturated solution. At both temperatures, the fast phase is unaffected by the CO concentration, whereas the long time tail of the kinetics is sensitive to this parameter and becomes slower as the CO concentration is reduced. This is a reliable indication about the nature of the two phases, with the faster phase being attributable to intramolecular geminate rebinding and the slower to a diffusion-mediated bimolecular event. The amplitude of the geminate recombination increases at decreasing temperatures, suggesting that ligand escape to the solution is assisted by protein dynamics and has to overcome an activation barrier. In other words, rebinding to the heme is favored over the escape process when the temperature is lowered, due to the larger activation energy of the escape process (see Table 1).

Several kinetic steps can be distinguished within the geminate phase. To assess more quantitatively the number of kinetics phases, we have estimated the lifetime distributions associated with the rebinding kinetics, using the maximum entropy method (MEM).[70,71] This method allows us to retrieve bias-free lifetime distributions associated with the CO rebinding kinetics. The presence of a kinetic phase in the progress curve appears in the lifetime distribution as a band. The advantage of this numerical method is that there is no a priori assumption about the number and the shape of the bands in the lifetime distribution. Even from a simple visual inspection, it is possible to have a good estimate of the number of kinetic phases and reaction intermediates. This piece of information is then used in subsequent numerical analysis with the differential equations associated with the derived kinetic model (Scheme 1).

Figure 3 reports the results of the analysis with the MEM of the CO rebinding kinetics to COAHB1 solutions and gels soaked in an aqueous buffer. Panel A shows the fitted rebinding curves. Residuals are reported as panels C and D in the same figure. Lifetime distributions are reported in panel B. Analysis of the rebinding kinetics to AHb1 solutions and gels soaked in aqueous buffer reveals, on the short time scale, the presence of two distinct bands with peaks at $\tau \approx 30$ ns (1) and $\tau \approx 300$ ns (2) at 10 °C, respectively (Figure 3). We have already interpreted this finding as an indication of the existence of two distinct rebinding sites within the protein matrix,[53,59] as suggested by previous investigations on myoglobin and human hemoglobin A.[37,38,40,51,52] It is reasonable to assume that the band observed at ≈30 ns (1) is due to rebinding from primary docking sites located in the distal cavity of the heme, while the smaller band

TABLE 1: Microscopic Rate Constants for AHb1 from the Fit of the Flash Photolysis Data at 20 °C[a]

	gel[b] 0% gly		gel 80% gly		gel 100% gly	
rate const	k[c]	E_a (kcal/mol)	k[c]	E_a (kcal/mol)	k[c]	E_a (kcal/mol)
k_{-1} (10^6 s^{-1})	4.8		4.7		26	
k_2 (10^7 s^{-1})	5.0		1.5	3.1 ± 0.3	0.4	7.0 ± 0.3
k_{-2} (10^7 $M^{-1}s^{-1}$)	1.6	8.6 ± 0.5	2.0	6.9 ± 0.4	0.7	8 ± 1
k_b (s^{-1})	100	7 ± 1	116	7 ± 1	100	7 ± 1
k_{-b} (s^{-1})	690	6.8 ± 0.9	387	8 ± 1	340	7 ± 1
k_c (10^7 s^{-1})	1.16	2.3 ± 0.1	4.3		4	
k_{-c} (10^7 s^{-1})	0.52	5 ± 2	0.57	4.2 ± 0.3	0.51	2.4 ± 0.3
k_d (10^6 s^{-1})			3.0		3.2	4.5 ± 0.2
k_{-d} (10^6 s^{-1})			1.8	5.4 ± 0.3	1.2	8.4 ± 0.7
k_e (10^5 s^{-1})			2	3.7 ± 1.5	4	
k_{-e} (10^5 s^{-1})			1.1	8.4 ± 0.8	2.9	

[a] Activation energies E_a were estimated from the linear Arrhenius plots for each rate constant k_i in the temperature range 10−40 °C. [b] Reevaluation of data from ref 53. [c] Error bars on the rate constants, determined from separate experimental data sets, are below 10% for all rates.

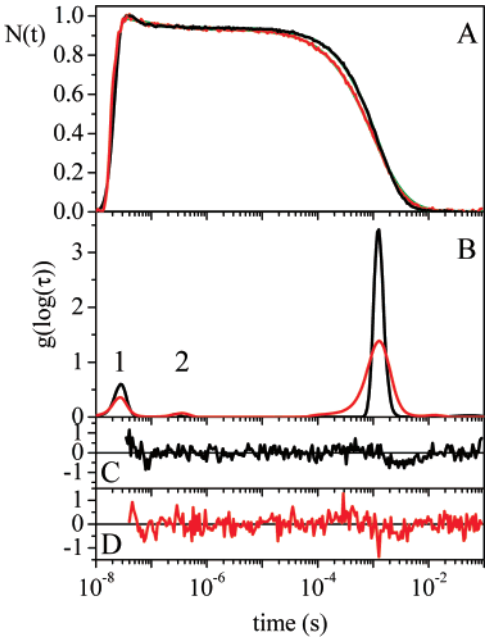

Figure 3. (A) Fittings obtained with the MEM (green curves) of the CO rebinding kinetics after photolysis of COAHb1 solutions (black curve) and COAHb1 gels soaked in a buffered solution (red curve) at $T = 10$ °C and 1 atm CO. (B) Lifetime distributions retrieved from fitting with the MEM in panel A (color code as in panel A). (C) and (D) show the residuals of the fittings on a ×50 scale (color code as in panel A).

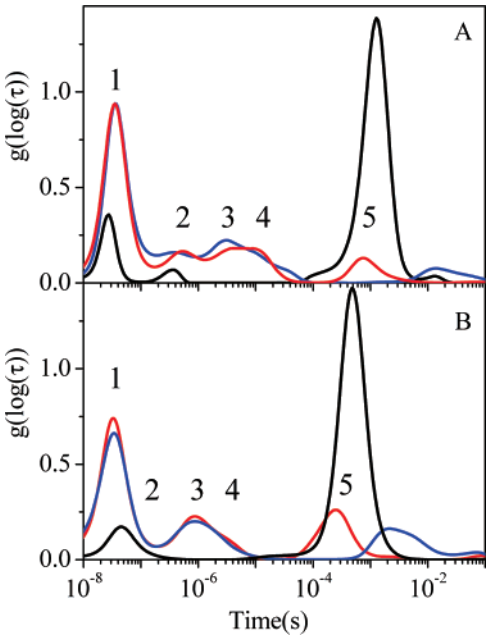

Figure 4. Lifetime distributions obtained with the MEM for the CO rebinding kinetics after photolysis of COAHb1 gels soaked in a buffered aqueous solution (black curve), in 100% glycerol at 1 atm CO (red curve) and in nitrogen-saturated 100% glycerol (blue curve): panel A, $T = 10$ °C; panel B, $T = 40$ °C.

SCHEME 1: Minimal Reactions for the Observed Kinetics with Sequential Migration between Internal Hydrophobic Cavities[a]

$$(Hb_p:CO)_2 \underset{k_{-d}}{\overset{k_d}{\rightleftarrows}} (Hb_p:CO)_3 \underset{k_{-e}}{\overset{k_e}{\rightleftarrows}} (Hb_p:CO)_4$$
$$k_c \uparrow\downarrow k_{-c}$$
$$HbCO \underset{k_{-1}}{\overset{h\nu}{\rightleftarrows}} (Hb_p:CO)_1 \underset{k_{-2}}{\overset{k_2}{\rightleftarrows}} Hb_p + CO$$
$$k_{-b} \uparrow\downarrow k_b$$
$$Hb_h + CO$$

[a] After photodissociation of the CO complex of AHb1 (HbCO), the photodissociated ligand can migrate to a primary docking site (Hb_p:$CO)_1$, from which it can sequentially access three secondary sites (Hb_p:$CO)_2$, (Hb_p:$CO)_3$, and (Hb_p:$CO)_4$ or exit to the solvent (Hb_p). The deoxy 5c-HS species (Hb_p) is in equilibrium with the deoxy 6c-LS species (Hb_h).

centered at ≈300 ns (2) is likely due to rebinding from a secondary site, located farther from the heme.

When the viscosity is increased by adding glycerol to the soaking solution, the progress curve clearly highlights a multiphasic pattern (Figures 1 and 2), which can be due to ligand migration through internal cavities. As observed for other hemoglobins,[40,41,48,50,52,56] the geminate rebinding is strongly enhanced, thus increasing sensitivity to internal processes.

Fitting of the rebinding kinetics with the MEM afforded very good results in all cases, with the fitted curves perfectly overlapping to the experimental data. Residuals were invariably small and randomly distributed around zero. The lifetime distributions retrieved from the analysis with the MEM of the rebinding curves to AHb1 gels soaked in 100% glycerol show structured bands associated with geminate recombination, with distinct peaks at approximately 30 ns (1), 500 ns (2), 3 μs (3), and 10 μs (4) at 10 °C (see Figure 4A). These peaks show very little sensitivity to the CO concentration. This finding is a more quantitative proof of the unimolecular nature of these processes. The shape of the lifetime distribution for the geminate rebinding is indicative of several distinct kinetics phases, with the fastest reaction reasonably attributed to the rebinding from primary docking sites inside the distal heme pocket. The temperature dependences of the shape and amplitude of these bands suggest that these kinetic steps have remarkable activation energy. While at 10 °C four distinct bands can be identified in the MEM distributions for CO rebinding to AHb1 gels soaked in 100%

glycerol (red and blue curves in Figure 4A), only three bands appear to contribute at higher temperatures (40 °C, red and blue curves in Figure 4B). The major peak at 30 ns (band 1 in Figure 4A) has a temperature-dependent amplitude and position (shifts to 48 ns at 40 °C) in the range 10−40 °C. This peak is characterized by an enhanced amplitude with respect to the corresponding peak obtained from the MEM analysis of CO rebinding kinetics to AHb1 gels in an aqueous buffer (black curves in Figure 4).[53] The first straightforward conclusion that can be drawn from this analysis is that rebinding from the primary docking site inside the distal heme pocket is greatly increased.

The other bands associated with the geminate recombination appear to reflect thermal activation, with band 2 likely merging into band 1 and the remainder bands (3 and 4) shifting to shorter lifetimes. Assuming that these bands reflect rebinding from internal hydrophobic cavities to which the photodissociated ligand has migrated, it seems appropriate to expect that these processes will display temperature- and viscosity-dependent efficiencies and rates. Thus, the apparent inverse temperature dependence of the kinetics in Figure 2 can be rationalized by assuming the existence of thermally activated migration processes from the primary docking site to other internal cavities and to the solution. As observed for other hemoglobins, the increase in temperature allows easier escape to solution, resulting in a larger amplitude of the slowest phase as the temperature is increased (Figure 2).

Rebinding kinetics measured at different CO partial pressures demonstrate that, even under high viscosity conditions, the photodissociated ligands still escape out of the protein matrix (possibly through the open tunnel which was detected in the structure determined by homology modeling[59]), although this process occurs with a dramatically reduced efficiency (Figures 1 and 2). The concentration dependence of the peak of band 5 (750 μs at 1 atm CO and 14 ms in a nitrogen-saturated solution, 10 °C) clearly demonstrates that this is a second-order process, thus confirming the fact that photodissociated CO can escape the protein matrix under these experimental conditions. In agreement with this, the process appears to have substantial thermal activation, with apparent lifetimes increasing to 250 μs and 2 ms when temperature is increased to 40 °C, at 1 atm CO and in a nitrogen-saturated solution, respectively. The second-order recombination bands are much broader in the gel than they are in solution, and this has been interpreted kinetically as arising from a more efficient competition of the distal HisE7 for binding to the heme Fe.[53] However, heterogeneity cannot be ruled completely out, and it may contribute to some extent. When viscosity is increased by bathing the gel in glycerol/water mixtures or in pure glycerol, the amplitude of the second-order band is decreased dramatically, accounting for approximately 10% in pure glycerol at 10 °C.

The above qualitative description arising from the lifetime distributions suggests possible reaction schemes to model the observed kinetics. The photodissociated ligand appears to migrate to a series of internal temporary docking sites from which it is rebound with different rates at later times.

The system of cavities through which the ligand appears to migrate can be tentatively identified from the three-dimensional structure model built by homology modeling.[59] The primary docking site is likely located within cavity **2** in Figure 5, on the distal side. Rebinding from this site is responsible for the 30 ns band at 10 °C in 100% glycerol (band 1 in Figure 4). The cavities labeled **1**, **3**, and **4** in Figure 5 are good candidates to host the additional secondary binding sites for the photodissociated ligand, but a more precise attribution of the observed kinetic phases to specific molecular events (or, equivalently, a precise identification of the temporary docking sites) is not possible at the present stage.

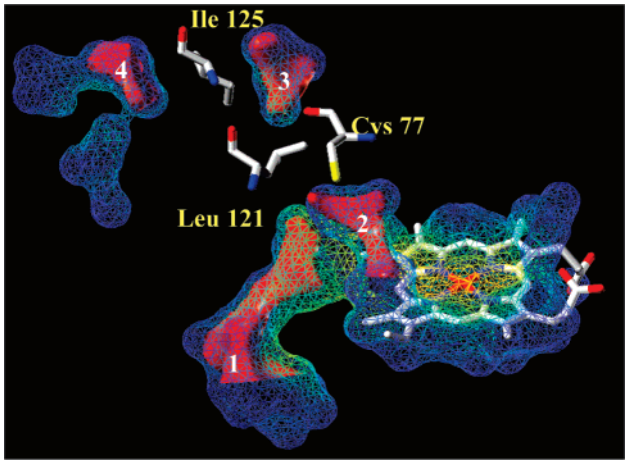

Figure 5. Close-up of the AHb1 internal cavities network in the model built by homology modeling. The heme group and the critical residues, regulating the communication between the different cavities, are displayed in capped sticks. Cavities **1**−**4** are represented by Connolly surface lines, colored as a function of the cavity depth. The opaque red contours identify the energetically and sterically favorable Xe sites, detected by the program GRID.[59]

We have recently shown that a simple branched kinetic scheme is capable of accounting for the observed CO rebinding kinetics in AHb1 solutions and COAHb1 gels.[53,59] Starting from those results, we have extended the model to account for multiple geminate kinetics phases. Several other reaction schemes were tested, but at the present level of accuracy, reaction Scheme 1 allowed us to obtain the best fits of the CO rebinding kinetics to AHb1 gels, with microscopic rates showing reasonably regular viscosity and temperature dependences. The differential equations associated with Scheme 1 were solved numerically and the solution was fitted to the experimental curve by optimizing the microscopic rates. Scheme 1 assumes that the photodissociated ligand can migrate from the distal heme pocket through a series of interconnected temporary sites, from which the ligand can be rebound at later times. Competition between migration and escape to the solvent phase determines the extent of the geminate recombination. The presence of the competitive reaction with the internal His ligand is also taken into account, but given the low rates for this process, the competition occurs only after the photodissociated ligand has escaped to solution.

Figure 6 reports sample fits of experimental data with the numerical solution of the differential equations associated with Scheme 1. The selected data reported in Figure 6 refer to COAHb1 gels soaked in 100% glycerol, either in equilibrium with 1 atm CO or purged with nitrogen, at 10 and 40 °C. The global analysis was performed on samples at the same temperature and bathed in solutions with the same glycerol concentration, equilibrated with 1 atm CO, 0.1 atm CO, and saturated with pure nitrogen. The fit is very good in all cases (see sample curves in Figure 6), and it further improves upon analyzing single rebinding curves. However, this improvement is detrimental to the rate constants which show less regular trends with temperature.

Figure 6 also reports the time courses of reaction intermediates. It can be clearly seen that the population of the kinetic traps inside the protein matrix is essentially independent of the CO partial pressure in the bathing solution, while temperature

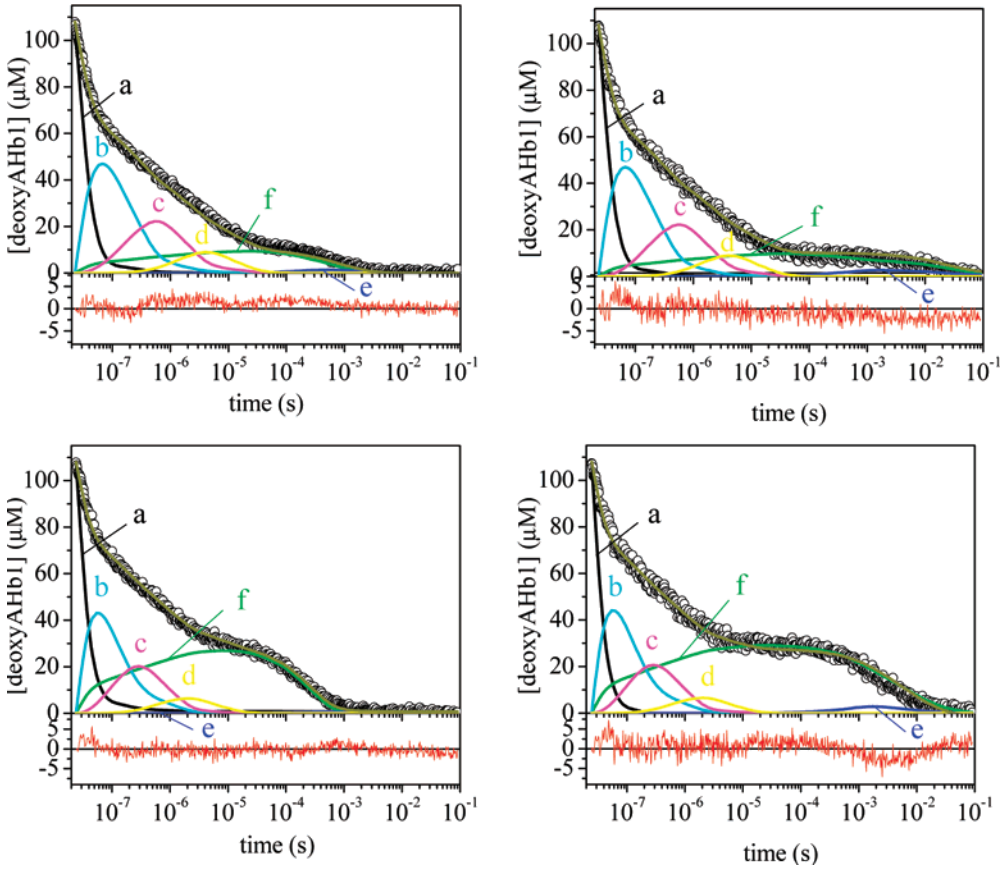

Figure 6. Selected curves from the global analysis of the CO binding kinetics to COAHb1 gels soaked in 100% glycerol saturated with 1 atm CO (left) and 1 atm N_2 (right), $T = 10$ °C (top) and $T = 40$ °C (bottom). The fits (dark yellow solid lines) are superimposed to the experimental data (circles). In the figures we have also reported the time course of the other relevant species in Scheme 1: $(Hb_p{:}CO)_1$ (black, a); $(Hb_p{:}CO)_2$ (cyan, b); $(Hb_p{:}CO)_3$ (magenta, c); $(Hb_p{:}CO)_4$ (yellow, d); Hb_h (blue, e); Hb_p (green, f). Residuals are reported in red in the bottom parts of each panel.

determines to a remarkable extent the concentration and the lifetime of each intermediate. In particular, the population of $(Hb_p{:}CO)_4$ (yellow line) reaches a maximum of ≈8% at 4 μs and is still appreciable up to 30 μs at 10 °C. This intermediate disappears in about 10 μs at 40 °C.

Table 1 reports the activation parameters determined from the linear Arrhenius plots of the microscopic rate constants (see Supporting Information) and the rate constants at 20 °C obtained from the fit. In the investigated temperature range, the innermost step (rate k_{-1}) is a barrierless process (or has a very small activation energy) under all experimental conditions, from aqueous solutions to gels soaked in 100% glycerol. The absence of a substantial activation barrier in the temperature range close to room temperature was previously observed for myoglobin,[38,41,74,75] human HbA,[51,52] and neuroglobin.[74,76] The rate k_{-1} is higher than that recently reported for myoglobin in silica gels ($\approx 10^6$ s^{-1}[38]) and more similar to what was found for human COHbA gels bathed in aqueous buffer solutions ($\approx 5 \times 10^6$ s^{-1} [51,52]). Still higher values were observed for human COHbA gels in the presence of 80% glycerol ($\approx 20 \times 10^6$ s^{-1} [51,52]).

The rate k_{-1} shows a substantial increase (≈×5) when COAHb1 gels are soaked in pure glycerol. Under these conditions the reduced water content of the gel pores is likely to affect the dynamics of solvation layer water molecules as well as the coupling between the protein dynamics and the solvent.[77,78] The use of glycerol to increase the effective viscosity on gel encapsulated proteins was first exploited by Friedman and co-workers to enhance the sensitivity of CO rebinding kinetics to geminate recombination.[54,79] The glycerol to water ratio was shown to have a clear effect on the relative amplitudes and onset of the kinetic phases,[38,50−52,54,79,80] suggesting that the coupling between the protein and the surrounding medium is modulated by the presence of the viscogenic agent. The very large increase in viscosity when glycerol approaches 100%[81] and the enormous effects observed on rebinding kinetics upon removal of residual hydration water from trehalose glasses[33,41,58,80] suggest that both viscosity and hydration contribute to the observed sharp increase in geminate recombination on going from 80% to 100% glycerol.

In the presence of glycerol, exit to the solvent phase (rate k_2) is a thermally activated process, with the activation energy apparently increasing when the glycerol concentration is increased. This is related, at least in part, to the decreased solubility of CO as glycerol concentration is increased.[50] Increasing glycerol concentration from 0 to 100% leads to a 10-fold decrease in this rate, thus favoring geminate rebinding over escape to solution. The concomitant 4-fold increase in the rate k_c is responsible for the population of reaction intermediates which extend the geminate recombination to longer times by trapping the photodissociated CO into temporary docking sites.

The 10-fold decrease in k_2, the 4-fold increase in k_c, and the 5-fold increase in k_{-1} explain the dramatic change in the amplitude and shape of the geminate recombination observed in the CO rebinding kinetics. Similar effects of glycerol on the amplitude of geminate recombination were observed for myoglobin,[38,40,41,50,80] hemoglobin,[50−52,54,82] and truncated hemoglobins.[56]

The activation energy for rebinding from the solvent phase (rate k_{-2}) is scarcely affected by glycerol concentration, with

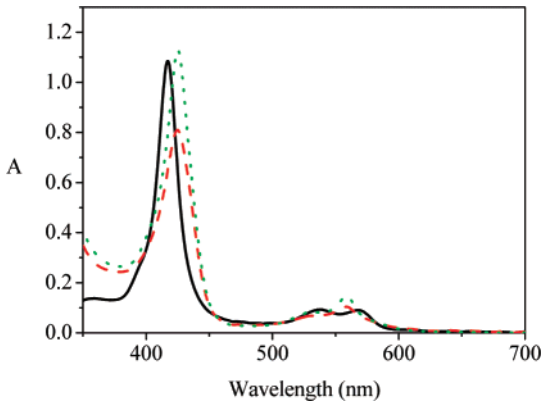

Figure 7. Absorption spectra of COAHb1 gels (black solid line), Fe^{2+} deoxy AHb1 gels obtained after photolysis of the COAHb1 gels (red dashed line), and Fe^{2+} deoxyAHb1 solution (green dotted line). [AHb1] = 143 μM, T = 20 °C, and pH = 7.

the rate at 20 °C decreasing by a factor 2 when the aqueous buffer is replaced by pure glycerol.

The small amplitude of the second-order recombination phase makes more difficult the detection of the competitive reaction (rate k_b) for Fe binding by the endogenous HisE7 ligand for COAHb1 gels in glycerol. These parameters are therefore determined with a much smaller precision from the numerical analysis. To improve the confidence on the parameters retrieved for the HisE7 ligation/deligation, we have estimated the ratio of 5c-HS to 6c-LS species in the Fe^{2+} deoxy state by measuring the absorbance spectrum in the gel. COAHb1 gels were photolyzed (and thus converted to Fe^{2+} deoxy species) by exposing the samples to white light for 5−20 min immediately before the spectra were collected. As shown for human hemoglobin, tertiary and quaternary transitions in the gel occur on a much longer time scale, thus allowing for the detection of an unliganded form that retains the conformation of the protein in the CO complex. The corresponding absorption spectra are reported in Figure 7. The ratio of 5c-HS to 6c-LS species was estimated by using the spectrum of the HE7L mutant (a detailed characterization of this mutated protein will be the subject of a future publication) as a reference for the fully 5c-HS form and the spectrum of nonsymbiotic hemoglobin AHb2 from *A. thaliana*[59] as a reference for the fully hexacoordinated one. The spectrum of the photolyzed sample encapsulated as CO complex shows a predominance of the 5c-HS ligation state, the 6c-LS form being only around 13%. This can be compared to the value determined for AHb1 solutions, for which we estimated 61% of the 6cLS species is present.[59] The difference in 6cLS species content can be directly appreciated by the comparison in Figure 7 between the solution absorption spectrum of deoxy Fe^{2+} AHb1 (green line) and the absorption spectrum of photolyzed COAHb1 gels (red line). Using this additional piece of information, the reevaluation of the microscopic rate constants for the CO rebinding to AHb1 solutions (Table 1) did not lead to substantial changes in the short time scale with respect to the previous analysis,[53] except for slightly lower values for rates k_{-1} and k_2 and a higher value for the rate k_{-c}. On the contrary, the parameters describing the competition between the HisE7 ligation and the CO binding from solution show a qualitatively different picture, consistent with equilibrium data from the optical absorbance spectra (Figure 7).

When COAHb1 gels were bathed in glycerol, we were not able to obtain substantial photolysis and the estimate of the ratio of 5c-HS to 6c-LS concentrations was not possible. The absorbance spectra of the deoxy Fe^{2+} AHb1 gels were used to obtain a qualitative evaluation of the equilibrium 5c-HS ⇌ 6c-LS. This estimate is subject to a possible systematic error as encapsulation of the protein in the deoxy Fe^{2+} state may trap different conformations with respect to the one obtained with COAHb1. The similarity between the spectra measured for the deoxy forms of AHb1 gels soaked in buffered solution and in glycerol suggests that the equilibrium between 5c-HS and 6c-LS species is similar under these conditions.

The activation energies reported in Table 1 were estimated from the Arrhenius plots which, in the investigated temperature range, were linear. The limited temperature covered by the present investigation does not allow one to highlight deviations from linearity, which become normally apparent when kinetic studies are extended to cryogenic temperatures.[13,83,84] With the present data it is difficult to assess the extent of slaving to solvent fluctuations of the various kinetic phases,[72,84] and experiments on more extended temperature ranges will be necessary to investigate this aspect. Nevertheless, we took advantage of the temperature dependence of viscosity for glycerol/water mixtures to track the coupling between solvent viscosity and protein dynamics, as previously done for myoglobin and hemoglobin.[50] We applied the modified Kramers equation which was proposed for those cases where reactions kinetics is influenced by protein dynamics and conformational changes.[16,17] Although Frauenfelder and co-workers observed that this expression fails to account for some experimental observations under extreme viscosity,[72] data in a regime of moderately high viscosity can be described appropriately.[16] Analysis of the experimentally determined microscopic rates within this model is reported as Supporting Information. In the case of k_{-2}, the activation energy obtained from the fit is 8 ± 1 kcal/mol, in agreement with the data reported in Table 1, with an internal viscosity σ = 40 cP. The agreement is slightly worse for k_2, and the best fit is obtained with an activation energy of 7 ± 1 kcal/mol, also in agreement with the data in Table 1, but with a much higher internal viscosity σ = 150 cP.

The presence of an internal source of friction for gel encapsulated proteins, not associated with the bulk viscosity, was recently demonstrated for MbCO and HbCO gels by Massari et al. using spectrally resolved infrared stimulated vibrational echo spectroscopy.[85] A comparison of the sol−gel experimental results to viscosity-dependent vibrational echo data taken on various mixtures of water and fructose showed that the gel encapsulated MbCO exhibits dynamics that are the equivalent to those observed for the same protein in a solution that is nearly 20 times more viscous than bulk water. In contrast, the HbCO dephasing in the gel was shown to be consistent with a 2-fold increase in viscosity. Using rotational correlation times for water previously reported,[86] Fayer and co-workers were also able to estimate that water confined to a length dimension of less than 2 nm is required to obtain the 45 cP aqueous environments estimated for the water surrounding gel encapsulated MbCO. Using the same procedure, it was estimated that gel encapsulated HbCO is surrounded by a layer of water that is 5 nm thick.

It is worthwhile to mention that we used the nominal bulk viscosity of the glycerol mixtures at the various temperatures. This parameter may contain some systematic error since it is hard to prevent small water contaminations in pure glycerol coming from residual water molecules trapped in the gel pores, which may cause an appreciable but hard to estimate change in viscosity.[81]

Even within the limited temperature/viscosity range investigated we believe our data give some insight into the ligand

migration mechanistics, which have possibly some relevance to the physiological role of the protein. The very complex kinetic pattern in the geminate phase is in keeping with the existence of migration of the photodissociated ligand between cavities. The accumulation, to an appreciable extent, of transient intermediates in which CO is docked in discrete positions gives access to possible functional mechanisms, where these states may be involved. Due to the combination of microscopic rates and activation energies, photodissociated ligands are stored temporarily in the internal cavities and are then rebound at longer times. These sites may likely act as a reservoir of the ligand, storing it for much longer times than it would be possible in the absence of migration through these cavities. For instance, the stored fraction in the state $(Hbp:CO)_4$ (yellow line) accounts for ≈8% of photodissociated ligands, up to a few microseconds (the maximum concentration of this species is observed at $t = 4\ \mu s$) after photolysis of COAHb1 samples at 10 °C and 1 atm CO.

The system of cavities allowing for internal mobility of ligands might be involved in the NO dioxygenase activity proposed for AHb1.[64] The reaction requires the sequential binding of two substrates, NO and O_2, to the heme. Secondary binding sites could contribute to the regulation of the multisubstrate reaction and to the confinement of unstable intermediates. In the case of neuroglobin,[62] truncated hemoglobins,[63] and myoglobin,[46] the metabolism of NO to nitrate seems to be accomplished through docking of NO to an internal cavity, until oxygen is bound to the heme Fe. In the case of AHb1, the presence of the kinetic traps gives ground to the hypothesis that the NO dioxygenase activity takes advantage of a similar system of cavities. The characterization of the accessibility of these docking sites and the reactivity of each intermediate is a fundamental step in gaining insight into the possible involvement of these reactant reservoirs in the metabolism of NO. Further experiments on NO and O_2 ligand rebinding are in progress, and the analysis of the complex kinetics observed for those reactants is expected to profit from the mechanistic insight provided by the present investigation.

Acknowledgment. We acknowledge the MIUR (PRIN2004) for financial support. P. J. Steinbach is kindly acknowledged for the use of Memexp.

Supporting Information Available: Arrhenius plots and viscosity dependence of microscopic rate constants. This material is available free of charge via the Internet at http://pubs.acs.org.

References and Notes

(1) Brunori, M.; Vallone, B. *FASEB J.* **2006**, *20*, 2192−2197.
(2) Ascenzi, P.; Bocedi, A.; deSanctis, D.; Pesce, A.; Bolognesi, M.; Marden, M. C.; Dewilde, S.; Moens, L.; Hankeln, T.; Burmester, T. *Biochem. Mol. Biol. Ed.* **2004**, *32*, 305−313.
(3) Wittenberg, J. B.; Bolognesi, M.; Wittenberg, B. A.; Guertin, M. *J. Biol. Chem.* **2002**, *277*, 871−874.
(4) Hunt, P. W.; Watts, R. A.; Trevaskis, B.; Llewelyn, D. J.; Burnell, J.; Dennis, E. S.; Peacock, W. J. *Plant Mol. Biol.* **2001**, *47*, 677−692.
(5) Austin, R. H.; Beeson, K.; Eisenstein, L.; Frauenfelder, H.; Gunsalus, I. C.; Marshall, V. P. *Science* **1973**, *181*, 541−543.
(6) Austin, R. H.; Beeson, K. W.; Eisenstein, L.; Frauenfelder, H.; Gunsalus, I. C. *Biochemistry* **1975**, *14*, 5355−5373.
(7) Huang, J.; Ridsdale, A.; Wang, J.; Friedman, J. M. *Biochemistry* **1997**, *36*, 14353−14365.
(8) Campbell, B. F.; Chance, M. R.; Friedman, J. M. *Science* **1987**, *238*, 373−376.
(9) Agmon, N. *Biochemistry* **1988**, *27*, 3507−3511.
(10) Steinbach, P. J. *Biochemistry* **1991**, *30*, 3988−4001.
(11) Doster, W.; Kleinert, T.; Post, F.; Settles, M. In *Protein-Solvent Interactions*; Gregory, R. B., Ed.; Marcel Dekker: New York, 1993; pp 375.
(12) Agmon, N.; Doster, W.; Post, F. *Biophys. J.* **1994**, *66*, 1612−1622.
(13) Kleinert, T.; Doster, W.; Leyser, H.; Petry, W.; Schwarz, V.; Settles, M. *Biochemistry* **1998**, *37*, 717−733.
(14) Beece, D.; Eisenstein, L.; Frauenfelder, H.; Good, D.; Marden, M. C.; Reinisch, L.; Reynolds, A. H.; Sorensen, L. B.; Yue, K. T. *Biochemistry* **1980**, *19*, 5147−5157.
(15) Agmon, N.; Hopfield, J. *J. Chem. Phys.* **1983**, *79*, 2042−2053.
(16) Ansari, A.; Jones, C. M.; Henry, E. R.; Hofrichter, J.; Eaton, W. *Science* **1992**, *256*, 1796−1798.
(17) Ansari, A.; Jones, C. M.; Henry, E. R.; Hofrichter, J.; Eaton, W. *Biochemistry* **1994**, *33*, 5128−5145.
(18) Powers, L.; Chance, B.; Chance, M.; Campbell, B.; Friedman, J.; Khalid, S.; Kumar, C.; Naqui, A.; Reddy, K. S.; Zhou, Y. *Biochemistry* **1987**, *26*, 4785−4796.
(19) Srajer, V.; Reinisch, L.; Champion, P. M. *Biochemistry* **1991**, *30*, 4886−4895.
(20) Schoenborn, B. P. *Nature* **1965**, *208*, 760−762.
(21) Tilton, R. F. J.; Kuntz, I. D. J.; Petsko, G. A. *Biochemistry* **1984**, *23*, 2849−2857.
(22) Schlichting, I.; Berendzen, J.; Phillips, G. N.; Sweet, R. M. *Nature* **1994**, *371*, 808−812.
(23) Hartmann, H.; Zinser, S.; Komninos, P.; Schneider, R. T.; Nienhaus, G. U.; Parak, F. *Proc. Natl. Acad. Sci. U.S.A.* **1996**, *93*, 7013−7016.
(24) Vojtechovsky, J.; Chu, K.; Berendzen, J.; Sweet, R. M.; Schlichting, I. *Biophys. J.* **1999**, *77*, 2153−2174.
(25) Ostermann, A.; Washipky, R.; Parak, F. G.; Nienhaus, G. U. *Nature* **2000**, *404*, 205−208.
(26) Brunori, M.; Vallone, B.; Cutruzzolà, F.; Travaglini-Allocatelli, C.; Berendzen, J.; Chu, K.; Sweeti, R. M.; Schlichting, I. *Proc. Natl. Acad. Sci. U.S.A.* **2000**, *97*, 2058−2063.
(27) Srajer, V.; Ren, Z.; Teng, T. Y.; Schmidt, M.; Ursby, T.; Bourgeois, D.; Pradervand, C.; Schildkamp, W.; Wulff, M.; Moffat, K. *Biochemistry* **2001**, *40*, 13802−13815.
(28) Bourgeois, D.; Vallone, B.; Schotte, F.; Arcovito, A.; Miele, A. E.; Sciara, G.; Wulff, M.; Anfinrud, P.; Brunori, M. *Proc. Natl. Acad. Sci. U.S.A.* **2003**, *100*, 8704−8709.
(29) Schotte, F.; Lim, M.; Jackson, T. A.; Smirnov, A. V.; Soman, J.; Olson, J. S.; Jr., G. N. P.; Wulff, M.; Anfinrud, P. A. *Science* **2003**, *300*, 1944−1947.
(30) Brunori, M.; Cutruzzolà, F.; Savino, C.; Travaglini-Allocatelli, C.; Vallone, B.; Gibson, Q. H. *Biophys. J.* **1999**, *76*, 1259−1269.
(31) Scott, E. E.; Gibson, Q. H. *Biochemistry* **1997**, *36*, 11909−11917.
(32) Scott, E. E.; Gibson, Q. H.; Olson, J. S. *J. Biol. Chem.* **2001**, *276*, 5177−5188.
(33) Librizzi, F.; Viappiani, C.; Abbruzzetti, S.; Cordone, L. *J. Chem. Phys.* **2002**, *116*, 1193−1200.
(34) Dantsker, D.; Samuni, U.; Friedman, A. J.; Yang, M.; Ray, A.; Friedman, J. M. *J. Mol. Biol.* **2002**, *315*, 239−251.
(35) Nienhaus, K.; Deng, P.; Kriegl, J. M.; Nienhaus, G. U. *Biochemistry* **2003**, *42*, 9647−9658.
(36) Nienhaus, K.; Deng, P.; Kriegl, J. M.; Nienhaus, G. U. *Biochemistry* **2003**, *42*, 9633−9646.
(37) Tetreau, C.; Blouquit, Y.; Novikov, E.; Quiniou, E.; Lavalette, D. *Biophys. J.* **2004**, *86*, 435−447.
(38) Sottini, S.; Abbruzzetti, S.; Viappiani, C.; Ronda, L.; Mozzarelli, A. *J. Phys. Chem. B* **2005**, *109*, 19523−19528.
(39) Abbruzzetti, S.; Giuffrida, S.; Sottini, S.; Viappiani, C.; Cordone, L. *Cell Biochem. Biophys.* **2005**, *43*, 431−438.
(40) Dantsker, D.; Roche, C.; Samuni, U.; Blouin, G.; Olson, J. S.; Friedman, J. M. *J. Biol. Chem.* **2005**, *280*, 38740−38755.
(41) Dantsker, D.; Samuni, U.; Friedman, J. M.; Agmon, N. *Biochim. Biophys. Acta* **2005**, *1749*, 234−251.
(42) Tian, W. D.; Sage, J. T.; Srajer, V.; Champion, P. M. *Phys. Rev. Lett.* **1992**, *68*, 408−411.
(43) Lim, M.; Jackson, T. A.; Anfinrud, P. A. *Proc. Natl. Acad. Sci. U.S.A.* **1993**, *90*, 5801−5804.
(44) Bourgeois, D.; Vallone, B.; Arcovito, A.; Sciara, G.; Schotte, F.; Anfinrud, P. A.; Brunori, M. *Proc. Natl. Acad. Sci. U.S.A.* **2006**, *103*, 4924−4929.
(45) Brunori, M.; Gibson, Q. H. *EMBO Rep.* **2001**, *2*, 674−679.
(46) Brunori, M. *TIBS* **2001**, *26*, 209−210.
(47) Bettati, S.; Pioselli, B.; Campanini, B.; Viappiani, C.; Mozzarelli, A. In *Encyclopedia of Nanoscience and Nanotechnology*; Nalwa, H. S., Ed.; American Scientific Publishers: Valencia, CA, 2004; Vol. 9, pp 81−103.
(48) Abbruzzetti, S.; Viappiani, C.; Bruno, S.; Mozzarelli, A. *Chem. Phys. Lett.* **2001**, *346*, 430−436.
(49) Abbruzzetti, S.; Viappiani, C.; Bruno, S.; Bettati, S.; Bonaccio, M.; Mozzarelli, A. *J. Nanosci. Nanotechnol.* **2001**, *1*, 407−415.

(50) Sottini, S.; Viappiani, C.; Ronda, L.; Bettati, S.; Mozzarelli, A. *J. Phys. Chem. B* **2004**, *108*, 8475−8484.
(51) Sottini, S.; Abbruzzetti, S.; Viappiani, C.; Bettati, S.; Ronda, L.; Mozzarelli, A. *J. Phys. Chem. B* **2005**, *109*, 11411−11413.
(52) Sottini, S.; Abbruzzetti, S.; Spyrakis, F.; Bettati, S.; Ronda, L.; Mozzarelli, A.; Viappiani, C. *J. Am. Chem. Soc.* **2005**, *127*, 17427−17432.
(53) Abbruzzetti, S.; Bruno, S.; Faggiano, S.; Grandi, E.; Mozzarelli, A.; Viappiani, C. *Photochem. Photobiol. Sci.* **2006**, *5*, 1109−1120.
(54) Khan, I.; Shannon, C. F.; Dantsker, D.; Friedman, A. J.; Perez-Gonzales-de-Apodaca, J.; Friedman, J. M. *Biochemistry* **2000**, *39*, 16099−16109.
(55) Samuni, U.; Dantsker, D.; Khan, I.; Friedman, A. J.; Peterson, E.; Friedman, J. M. *J. Biol. Chem.* **2002**, *277*, 25783−25790.
(56) Samuni, U.; Dantsker, D.; Ray, A.; Wittenberg, J. B.; Wittenberg, B. A.; Dewilde, S.; Moens, L.; Ouellet, Y.; Guertin, M.; Friedman, J. M. *J. Biol. Chem.* **2003**, *278*, 27241−27250.
(57) Samuni, U.; Roche, C. J.; Dantsker, D.; Juszczak, L. J.; Friedman, J. M. *Biochemistry* **2006**, *45*, 2820−2835.
(58) Cordone, L.; Cottone, G.; Giuffrida, S.; Palazzo, G.; Venturoli, G.; Viappiani, C. *Biochim. Biophys. Acta* **2005**, *1749*, 252− 281.
(59) Bruno, S.; Faggiano, S.; Spyrakis, F.; Mozzarelli, A.; Abbruzzetti, S.; Grandi, E.; Viappiani, C.; Feis, A.; Mackowiak, S.; Smulevich, G.; Cacciatori, E.; Dominici, P. *J. Am. Chem. Soc.* **2007**, *129*, 2880−2889.
(60) Pesce, A.; Dewilde, S.; Nardini, M.; Moens, L.; Ascenzi, P.; Hankeln, T.; Bolognesi, T. B. *Structure* **2003**, *11*, 1087−1095.
(61) Vallone, B.; Nienhaus, K.; Matthes, A.; Brunori, M.; Nienhaus, G. U. *Proc. Natl. Acad. Sci. U.S.A.* **2004**, *101*, 17351−17356.
(62) Brunori, M.; Giuffrè, A.; Nienhaus, K.; Nienhaus, G. U.; Scandurra, F. M.; Vallone, B. *Proc. Natl. Acad. Sci. U.S.A.* **2005**, *102*, 8483−8488.
(63) Bidon-Chanal, A.; Martí, M. A.; Crespo, A.; Milani, M.; Orozco, M.; Bolognesi, M.; Luque, F. J.; Estrin, D. A. *Proteins* **2006**, *64*, 457−464.
(64) Perazzolli, M.; Dominici, P.; Puertas, M. C. R.; Zago, E.; Zeier, J.; Sonoda, M.; Lamb, C.; Delledonne, M. *Plant Cell* **2004**, *16*, 2785−2794.
(65) Perazzolli, M.; Romero-Puertas, M. C.; Delledonne, M. *J. Exp. Bot.* **2006**, *57*, 479−488.
(66) Shibayama, N.; Saigo, S. *J. Mol. Biol.* **1995**, *251*, 203−209.
(67) Bruno, S.; Bonaccio, M.; Bettati, S.; Rivetti, C.; Viappiani, C.; Abbruzzetti, S.; Mozzarelli, A. *Protein Sci.* **2001**, *10*, 2401−2407.
(68) Bettati, S.; Mozzarelli, A. *J. Biol. Chem.* **1997**, *272*, 32050−32055.
(69) Banderini, A.; Sottini, S.; Viappiani, C. *Rev. Sci. Instrum.* **2004**, *75*, 2257−2261.
(70) Steinbach, P. J. *J. Chem. Inf. Comput. Sci.* **2002**, *42*, 1476−1478.
(71) Steinbach, P. J.; Ionescu, R.; Matthews, C. R. *Biophys. J.* **2002**, *82*, 2244−2255.
(72) Frauenfelder, H.; Fenimore, P. W.; McMahon, B. H. *Biophys. Chem.* **2002**, *98*, 35−48.
(73) Bruno, S.; Faggiano, S.; Spyrakis, F.; Mozzarelli, A.; Cacciatori, E.; Dominici, P.; Grandi, E.; Abbruzzetti, S.; Viappiani, C. *Gene* **2007**, *398*, 224−233.
(74) Kriegl, J. M.; Bhattacharyya, A. J.; Nienhaus, K.; Deng, P.; Minkow, O.; Nienhaus, G. U. *Proc. Natl. Acad. Sci. U.S.A.* **2002**, *99*, 7992−7997.
(75) Agmon, N. *Int. J. Chem. Kinet.* **1981**, *13*, 333- 365.
(76) Nienhaus, K.; Kriegl, J. M.; Nienhaus, G. U. *J. Biol. Chem.* **2004**, *279*, 22944−22952.
(77) Navati, M. S.; Ray, A.; Shamir, J.; Friedman, J. M. *J. Phys. Chem. B* **2004**, *108*, 1321−1327.
(78) Roche, C. J.; Guo, F.; Friedman, J. M. *J. Biol. Chem.* **2006**, *281*, 38757−38768.
(79) Khan, I.; Dantsker, D.; Samuni, U.; Bonaventura, A. J. F.; Manjula, B.; Acharya, S. A.; Friedman, J. M. *Biochemistry* **2001**, *40*, 7581−7592.
(80) Samuni, U.; Dantsker, D.; Roche, C. J.; Friedman, J. M. *Gene* **2007**, *398*, 234−248.
(81) Sheely, M. L. *Ind. Eng. Chem.* **1932**, *24*, 1060−1064.
(82) Samuni, U.; Juszczak, L.; Dantsker, D.; Khan, I.; Friedman, A. J.; Perez-Gonzalez-de-Apodaca, J.; Bruno, S.; Hui, H. L.; Colby, J. E.; Karasik, E.; Kwiatkowski, L. D.; Mozzarelli, A.; Noble, R. W.; Friedman, J. M. *Biochemistry* **2003**, *42*, 8272−8288.
(83) Iben, I. E. T.; Braunstein, D.; Doster, W.; Frauenfelder, H.; Hong, M. K.; Johnson, J. B.; Luck, S.; Ormos, P.; Schulte, A.; Steinbach, P. J.; Xie, A. H.; Young, R. D. *Phys. Rev. Lett.* **1989**, *62*, 1916−1919.
(84) Fenimore, P. W.; Frauenfelder, H.; McMahon, B. H.; Parak, F. G. *Proc. Natl. Acad. Sci. U.S.A.* **2002**, *99*, 16047−16051.
(85) Massari, A. M.; Finkelstein, I. K.; Fayer, M. D. *J. Am. Chem. Soc.* **2006**, *128*, 3990−3997.
(86) Tan, H. S.; Piletic, I. R.; Fayer, M. D. *J. Chem. Phys.* **2005**, *122*, 174501.